JGR Oceans

RESEARCH ARTICLE
10.1029/2024JC022222

Subsurface Cooling and Sea Surface Temperature Pattern Formation Over the Equatorial Pacific

Feng Jiang[1], Richard Seager[1], Mark A. Cane[1], Christina Karamperidou[2], and Noel G. Brizuela[1]

[1]Lamont-Doherty Earth Observatory, Columbia University, Palisades, NY, USA, [2]Department of Atmospheric Sciences, School of Ocean and Earth Science and Technology, University of Hawai'i at Mānoa, Honolulu, HI, USA

Key Points:

- Subsurface cooling is evident in observations and climate models in response to historical radiative forcing but with different features
- Models simulating the subsurface cooling most similar to observations best reproduce the historical sea surface temperature trend pattern
- Increased stability in the upper ocean of some models prevents subsurface cooling from being effectively communicated to the surface

Supporting Information:

Supporting Information may be found in the online version of this article.

Correspondence to:

F. Jiang,
fjiang@ldeo.columbia.edu

Citation:

Jiang, F., Seager, R., Cane, M. A., Karamperidou, C., & Brizuela, N. G. (2025). Subsurface cooling and sea surface temperature pattern formation over the equatorial pacific. *Journal of Geophysical Research: Oceans*, *130*, e2024JC022222. https://doi.org/10.1029/2024JC022222

Received 3 DEC 2024
Accepted 10 APR 2025

Author Contributions:

Conceptualization: Feng Jiang, Richard Seager, Mark A. Cane
Formal analysis: Feng Jiang
Investigation: Richard Seager, Noel G. Brizuela
Methodology: Feng Jiang, Richard Seager
Supervision: Richard Seager, Mark A. Cane
Writing – original draft: Feng Jiang
Writing – review & editing: Richard Seager, Mark A. Cane, Christina Karamperidou, Noel G. Brizuela

Abstract The equatorial cold tongue region has not warmed up in response to historical radiative forcing in the real world, contrary to the strong warming often simulated by climate models. Here we demonstrate that climate models fail to represent one or both of the key processes driving observed sea surface temperature (SST) pattern formation: a realistic surface wind stress pattern shaping subsurface cooling through wind-driven circulation changes, and effective connectivity between subsurface and surface temperatures via upwelling and mixing. Consequently, none of the models approximate the observed lack of cold tongue SST warming and strengthening of zonal SST gradient across the equatorial Pacific. Furthermore, those that come closest achieve this due to interhemispheric warming differences rather than equatorial dynamics as observed. Addressing different origins of subsurface cooling in observations and simulations, and how they connect to SST, will lead to improved understanding of tropical Pacific SST changes to date and how they will evolve in the future.

Plain Language Summary The observed subsurface cooling trend in the tropical Pacific upper ocean has been previously linked to the lack of sea surface temperature (SST) warming in the cold tongue region. Although climate models tend to simulate a warmer cold tongue under historical radiative forcing, they also prominently feature a subsurface cooling trend. In this study, we show that models simulating the subsurface cooling most similar to observations best reproduce the observed SST trend pattern. In models that simulate a same-signed response in zonal SST gradient as observed, the simulated subsurface cooling is driven mainly by wind-driven Ekman pumping changes, similar to observations. In models with opposite-signed response in zonal SST gradient, the deeper and more westward displaced subsurface cooling compared to that of observations is primarily linked to changes in meridional overturning circulation and subsurface mixing. We also explore the potential mechanisms affecting the efficiency of subsurface cooling in influencing SST pattern formation in both observations and model simulations based on quantifications of the Richardson number change and contributions from different processes involved.

1. Introduction

Although the response of tropical Pacific sea surface temperature (SST) and atmospheric circulation to radiative forcing has an extensive literature (Cane et al., 1997; Chung et al., 2019; Clement et al., 1996; Heede & Fedorov, 2021; Karamperidou et al., 2017; Olonscheck et al., 2020; Seager et al., 2019; Vecchi et al., 2006; Watanabe et al., 2021; Zhang et al., 2010), the changes in the upper ocean has received much less attention. This is despite the fact that the upper tropical Pacific Ocean undoubtedly influences SST and, hence, the atmospheric response. The zonal gradient of SST has strengthened across the equatorial Pacific over the past several decades, with pronounced warming in the western Pacific and a lack of warming or even cooling in the central-to-eastern Pacific (Cane et al., 1997; Coats & Karnauskas, 2018; Seager et al., 2022). The ocean dynamical thermostat (ODT) hypothesis has been proposed to explain this lack of warming in the equatorially confined upwelling region (Cane et al., 1997; Clement et al., 1996; Seager et al., 2019, 2022). The ODT posits that the surface warming in response to greenhouse gases (GHGs) in the cold tongue region can be offset by the enhanced vertical cold advection and ocean heat flux divergence, therefore resisting warming during the historical period. A deep thermocline, weak vertical temperature gradients, and weak winds and upwelling in the western Pacific mean the GHG-induced warming is not similarly offset and SSTs must warm by more. The differential warming rate between the western and eastern equatorial Pacific enhances the zonal SST gradient, which can sustain and amplify itself through Bjerknes feedback. Our recent work further demonstrates that the wind-driven cooling and

shoaling of the tropical Pacific Ocean thermocline over past decades, influences the central-to-eastern SST trend pattern through vertical feedback processes (Jiang et al., 2024a, Jiang et al., 2024b).

In contrast to observations, climate models from phases 3, 5, and 6 of Coupled Model Intercomparison Project (CMIP) as well as multiple Large Ensembles (LEs), preferentially simulate a weakened SST zonal gradient across the tropical Pacific, characterized by greater warming in the east than in the west (Lee et al., 2022; Olonscheck et al., 2020; Seager et al., 2019, 2022; Watanabe et al., 2024; Wills et al., 2022). There is an ongoing debate about whether this model-observation discrepancy arises from the influence of internal variability in the observations (Watanabe et al., 2021), or systematic biases within climate models (Seager et al., 2019). Our recent work suggests that the SST trend in the tropical Pacific since the late 1950s is unlikely to be strongly impacted by internal variability, particularly the Interdecadal Pacific Oscillation (Jiang et al., 2024a), lending support to model biases as the cause. Despite their tendency to warm the eastern SST, subsurface cooling remains a prominent feature across generations of climate model simulations subjected to radiative forcing (Ju et al., 2022; Seager et al., 2022; Watanabe et al., 2021). In response to increasing CO_2, climate models predict a local minimum in ocean warming near the central-to-western equatorial thermocline (Y. Luo, Liu, & Lu, 2018; Vecchi et al., 2006; Vecchi & Soden, 2007). Several mechanisms have been proposed to understand this subsurface cooling. Vecchi and Soden (2007) interpreted it as an equatorial ocean dynamical feedback process, where the thermocline tilt relaxes in response to weakened surface wind stress. The minimum warming in the central-to-western equatorial thermocline has also been linked to the slowdown in the Subtropical Cells (STCs), potentially driven by increased stratification of the upper ocean due to surface warming (Y. Luo et al., 2009, 2018; Y. Luo & Rothstein, 2011), or by reduced meridional subsurface convergence resulting from the weakening of the Walker circulation and the associated decrease in surface zonal wind stress over the equatorial Pacific (C. Yang et al., 2014; H. Yang et al., 2009). Furthermore, Ju et al. (2022) suggest that the "spiciness effect", referring to the density-compensated anomalies of temperature and salinity produced in the outcropping regions of the North and South Pacific through air-sea interaction and anomalous subduction (Munk, 1981; Schneider, 2000), also impacts the tropical subsurface ocean, leading to thermocline cooling via the STCs.

It is therefore puzzling that, although our previous studies argued that the observed lack of warming in the eastern Pacific SST is closely related to local subsurface cooling (Jiang et al., 2024a, Jiang et al., 2024b), the similar cooling in climate models does not appear to connect with the surface and strengthen the zonal SST gradient in the equatorial Pacific.

2. Materials and Methods

We analyze SST data from four observational data sets: the Hadley Center data HadISST version 1.1 (Rayner et al., 2003), the National Oceanic and Atmospheric Administration ERSSTv5 data (Huang et al., 2017), the Centennial in situ Observation Based Estimates (COBE) of SST from the Japanese Meteorological Agency (Ishii et al., 2005), and Kaplan Extended SST version 2 (Kaplan et al., 1998). This study primarily focuses on long-term SST trends over the period 1958–2022, which roughly corresponds to the period over which the warm pool has warmed (Jiang et al., 2024b; Seager et al., 2022). Additionally, we extend the SST trend analysis back to 1900 to assess the robustness of the long-term trend patterns. For subsurface temperature (T) data, we utilize two reanalysis data sets: the Ocean ReAnalysis System-5 (ORAs5) from the European Center for Medium-Range Weather Forecasts (Zuo et al., 2019) during 1958–2022, and the Simple Ocean Data Assimilation, version 2.2.4 (SODA2.2.4) (Carton & Giese, 2008) during 1958–2008. Two observational-only data sets including EN4 data (Good et al., 2013) during 1958–2022 and Ishii data during 1958–2012 (Ishii & Kimoto, 2009) are also utilized. The surface wind stress ($\boldsymbol{\tau}$), ocean salinity (Sa), and zonal (U) and meridional currents (V) from ORAs5 are also used to investigate subsurface ocean processes. For climate model simulations, we analyze outputs of SST, surface wind stress, subsurface temperature, and zonal and meridional currents from historical simulations spanning 1958 to 2014, extended to 2022 using the Shared Socioeconomic Pathways (SSP) 3–7.5 scenario (Eyring et al., 2016; O'Neill et al., 2016) from single-model initial condition LEs (Deser et al., 2020). The selection criteria for LEs require at least 10 ensemble members and the availability of subsurface temperature data in public archives. Detailed descriptions of the LE models used are provided in Table S1 in Supporting Information S1. Only LEs were used so that the forced response could be identified in each model.

All SST and surface wind stress data from observational data sets and LE simulations were re-gridded to a $1° \times 1°$ resolution for comparison. Subsurface temperature and ocean current data were re-gridded horizontally to $1° \times 1°$

and vertically to a 10 m equally spaced grid. For LE simulations, the forced response in each model was calculated as the trend in the multi-member mean and the multi-model mean forced trend was calculated as the average forced change across all LEs. Anomalies for all variables were determined as deviations from the monthly climatology during 1958–2022. Statistical significance tests were conducted using the two-tailed Student's *t*-test with an effective sample size of n-2. Significance tests were applied only to trend estimations. For composite analyses, significant tests were omitted due to the limited sample size in some cases (e.g., four observational data sets), and information for individual data sets is presented in either the scatterplot or the supplementary figures in Supporting Information S1.

To illustrate the oceanic processes related to the SST pattern formation, we calculated the Ekman pumping velocity (w_E) and Meridional Overturning Circulation (MOC) for observations and LE model simulations. w_E was derived from the divergence of the Ekman transport (Zebiak & Cane, 1987):

$$w_E = \nabla_H \cdot \boldsymbol{U_E} = \nabla_H \cdot \frac{r_s \boldsymbol{\tau} + f(\boldsymbol{\tau} \times \boldsymbol{k})}{\rho_0 \left(f^2 + {r_s}^2\right)}. \tag{1}$$

in which r_s is the surface layer friction coefficient (0.5 days^{-1}), f is the Coriolis parameter, $\boldsymbol{k}$ is the unit vector in the vertical direction, and ρ_0 is the reference ocean density (1,037 kg/m^3). This formulation allows w_E to be evaluated as f goes to zero.

The MOC (ψ) in the tropical Pacific was calculated as the stream function of the meridional currents:

$$\psi(\Phi, z) = \int_z^0 \int_{\lambda_W}^{\lambda_E} v cos\Phi d\lambda dz, \tag{2}$$

in which Φ is the latitude, λ the longitude, z the depth, and λ_E and λ_W are the eastern (90°W) and western (150°E) boundaries used in the MOC calculation.

We also quantify the stratification in the tropical Pacific Ocean as follows:

$$N^2 = -g\left(\alpha \frac{\partial T}{\partial z} + \beta \frac{\partial Sa}{\partial z}\right), \tag{3}$$

in which N is the Brunt-Väisälä frequency (buoyancy frequency), g is the acceleration of gravity (9.8 m/s^2), α is the thermal expansion coefficient (0.00021°C^{-1}), β is the haline contraction coefficient (−0.00074 PSU^{-1}). Note that in the historical period, changes in $\frac{\partial T}{\partial z}$ dominate observed stratification change in the tropical Pacific upper ocean (Li et al., 2020).

We then assess changes in mixing by calculating the gradient Richardson number (*Ri*) as follows:

$$Ri = \frac{N^2}{S^2} \tag{4}$$

in which S^2 indicates the vertical shear of horizontal currents, calculated as $\left(\frac{\partial U}{\partial z}\right)^2 + \left(\frac{\partial V}{\partial z}\right)^2$, and is dominated by $\left(\frac{\partial U}{\partial z}\right)^2$. However, the trend in *Ri* is not solely dependent on the trends in N^2 and S^2 but is also closely tied to their climatological values. To simplify, we frame our analysis around the change in *Ri* between two periods: P1 (1958–1977) and P2 (2003–2022), following our previous work (Jiang et al., 2024a, Jiang et al., 2024b). We define the period-average in P1 as the climatology (denoted by an overbar) and the difference between P2 and P1 as the anomaly (denoted by a prime). Thus, the change in *Ri* is expressed as follows:

$$Ri' = \frac{\overline{N^2} + N^{2\prime}}{\overline{S^2} + S^{2\prime}} - \frac{\overline{N^2}}{\overline{S^2}} \tag{5}$$

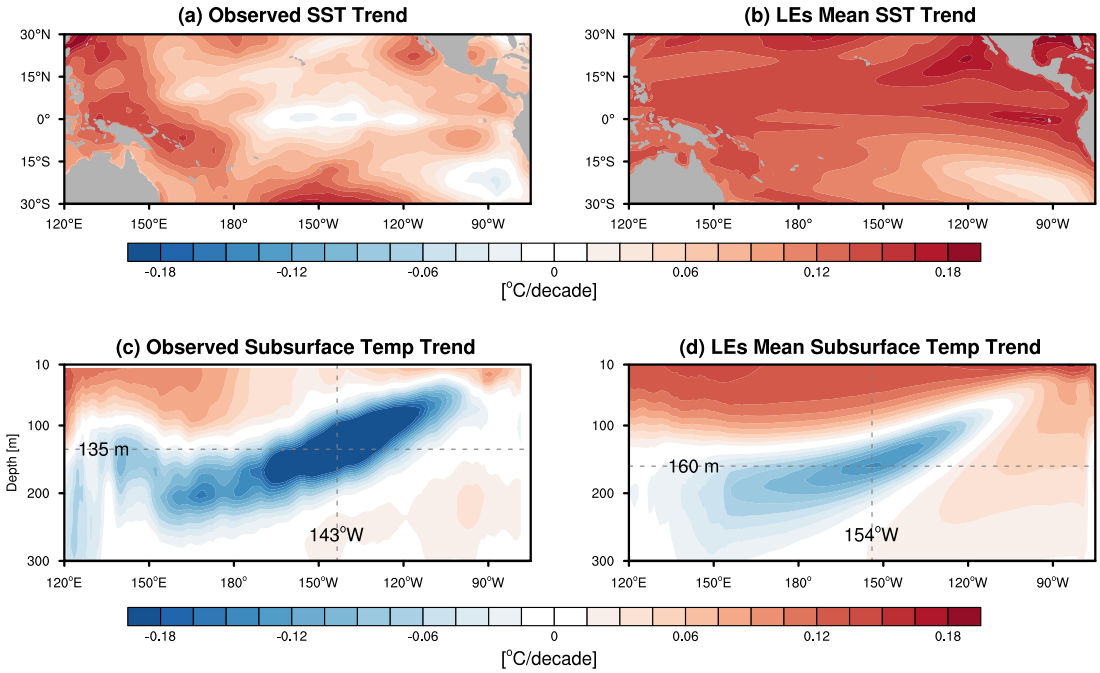

Figure 1. Trend in sea surface temperature (SST) and subsurface temperature for observation and Large Ensemble (LE) simulations. (a) Composited equatorial (5°S ~ 5°N) SST trend (°C/decade) during 1958–2022 based on HadISST, ERSSTv5, Centennial in Situ Observation Based Estimates, and Kaplan, (b) Composited equatorial forced SST trend (°C/decade) across 11 LEs (Table S1 in Supporting Information S1), (c) Composited equatorial subsurface temperature trend (°C/decade) based on ORAs5 (1958–2022), SODA2.2.4 (1958–2008), Ishii (1958–2012), and EN4 (1958–2022), and (d) composited equatorial forced subsurface temperature trend (°C/decade) across 11 LEs. The dashed lines in (c) and (d) indicate the depth and longitude of the maximum subsurface cooling.

Separating the Right-Hand-Side (RHS) terms related to changes in $N^{2\prime}, S^{2\prime}$ and the cross terms (Residual), Equation 5 can be written as follows:

$$Ri' = \overline{Ri}\frac{N^{2\prime}}{\overline{N^2}} - \overline{Ri}\frac{1}{\left(1+\frac{1}{S^{2\prime}/\overline{S^2}}\right)} - \overline{Ri}\frac{N^{2\prime}S^{2\prime}}{\overline{N^2}\left(\overline{S^2}+S^{2\prime}\right)} \tag{6}$$

in which the RHS terms are referred to as $Ri'_{N^{2\prime}}, Ri'_{S^{2\prime}}$ and Res respectively.

3. SST Trend Pattern and Subsurface Temperature Trend Structure in Observations and LEs

The meridionally confined lack of SST warming in the cold tongue region stands out against the widespread warming observed across much of the tropical oceans and, in particular against the pronounced warming over the tropical Pacific warm pool since the late 1950s (Figure 1a). This SST trend pattern with a strengthened zonal (west-minus-east) SST gradient across the equatorial Pacific is consistently identified in four observational data sets during 1958–2022 (Figures S1a–d in Supporting Information S1). This lack of warming persists robustly over longer periods dating back to 1,900 (Figures S1e–h in Supporting Information S1). This contrasts sharply with the majority of climate model simulations for the same historical period (Seager et al., 2019; Wills et al., 2022). As shown in Figure 1b, the multi-model mean forced response of SST across 11 LEs is characterized by a reduced SST gradient across the tropical Pacific.

The observed surface cooling in the cold tongue region has been demonstrated (Jiang et al., 2024a, Jiang et al., 2024b; Seager et al., 2022) to be closely associated with the subsurface cooling in the central-to-eastern Pacific near the thermocline but reaching up to the mixed layer roughly east of 140°W (Figure 1c). The multi-model mean forced response in subsurface temperature (Figure 1d) features an increased vertical temperature gradient from the surface to the thermocline with warming above and cooling below and a less pronounced east-west contrast compared to the observed trend (Figure 1c). The subsurface cooling in models is generally weaker,

displaced further west and deeper (as indicated by dashed lines in Figures 1c and 1d), and is accompanied by stronger warming in the upper layer relative to the observations. This raises the question of why subsurface cooling in climate models does not appear to affect cold tongue SST in the same way as observed.

Figure 2a shows the forced response in the zonal SST gradient across the equatorial Pacific as the SST trend difference between the western equatorial Pacific (5°S−5°N, 140°E−170°E) and the central-to-eastern equatorial Pacific (5°S−5°N, 170°W−90°W) for individual LEs. Of the 11 LEs analyzed, 4 models (E3SM-1-0, E3SM-2-0, MPI-ESM1-2-LR, and UKESM1-0-LL) simulate a strengthened zonal SST gradient, but its magnitude is significantly weaker than the observed trend. Even allowing for internal variability, very few individual simulations of these models come close to the observed trends (Figure 2a). Nevertheless, we refer to these LEs as "same-signed models" hereafter. In contrast, 6 models (ACCESS-ESM1-5, CanESM5, CanESM5-1, MPI-ESM1-2-HR, MIROC6, and MIROC-ES2L) simulate a weakening of the SST gradient across the equatorial Pacific. These are referred to as "opposite-signed models." IPSL-CM6A-LR shows a near-zero forced response in zonal SST gradient with relatively uniform zonal warming (Figure S2 in Supporting Information S1), and is excluded from classification.

Interestingly, the opposite-signed models display stronger subsurface cooling than the same-signed models (Figures 2d–2f). The opposite-signed models show a well-stratified vertical temperature trend structure with strong surface warming and also strong subsurface cooling (Figure 2d), in contrast to the weaker increase in vertical temperature gradient in the same-signed models (Figure 2e). As shown in Figure 2f, a negative relationship is observed across different LEs between forced response in the zonal SST gradient and the magnitude of subsurface cooling, with a correlation coefficient of −0.35 (not statistically significant at the 95% confidence level). The magnitude of subsurface cooling is defined by the intensity of the maximum cooling in the tropical Pacific upper ocean. Models that exhibit stronger subsurface cooling tend to simulate a weakened zonal SST gradient. This is the opposite of what would be expected if the subsurface cooling was driving the SST in the upwelling region and, hence, the SST gradient. In contrast, the observations have the most pronounced subsurface cooling but also the greatest strengthening of the zonal SST gradient, a relationship that stands apart from that in the models.

Instead, we find that it is the spatial structure of the equatorial subsurface cooling that matters for the SST trend pattern formation. There is a strong inverse relationship between the forced zonal SST gradient trend and the depth of the maximum subsurface cooling (Figure 2g; $R = -0.60$, significant at the 95% confidence level) and an even stronger positive relationship with the longitude of the subsurface cooling (Figure 2h; $R = 0.84$, significant at the 95% confidence level) in LEs. Models with subsurface cooling shallower and more eastward displaced are more likely to simulate a strengthened zonal SST gradient as observed. There is a positive relationship between the magnitude and depth of the cooling across models with a correlation coefficient of 0.72 (significant at the 95% confidence level), which likely contributes to the inverse relationship observed in Figure 2f. Moreover, the two metrics defining the spatial structure of the subsurface cooling are also not independent and have a correlation coefficient of 0.41, due to the subsurface cooling primarily occurring near the thermocline, which tilts up climatologically from west to east. Consequently, incorporating both spatial metrics in a multivariate reconstruction of equatorial SST gradient trend by multiple linear regression only marginally improves the explained variance from 71% when using the longitude of maximum cooling alone to 74% when including both variables. Note that all intermodel relationships presented here are based on a sample size of only 11 and may be subject to sampling error and uncertainty.

4. Dynamics Linking the Subsurface Temperature to Surface Wind Stress

As demonstrated in our recent work (Jiang et al., 2024b), the observed subsurface cooling in ORAs5 is driven by changes in surface wind stress and associated ocean dynamics. The observed increase in zonal wind stress over the central Pacific (west of 140°W) induces a significant increase in local Ekman pumping (Figure 3a), thereby cooling the thermocline where the climatological vertical temperature gradients are large (Figure 1c). In the eastern equatorial Pacific, the Ekman pumping change is weakly negative (Figure 3e). In the opposite-signed models, there is a notable weakening of zonal wind stress extending from near the dateline to the South American coast, accompanied by a broad reduction in Ekman pumping across the equatorial Pacific (Figure 3b and Figures S3a–S3f in Supporting Information S1). In the same-signed models, the zonal wind stress strengthens in the central Pacific and weakens in the east, a pattern that closely resembles observations but with different

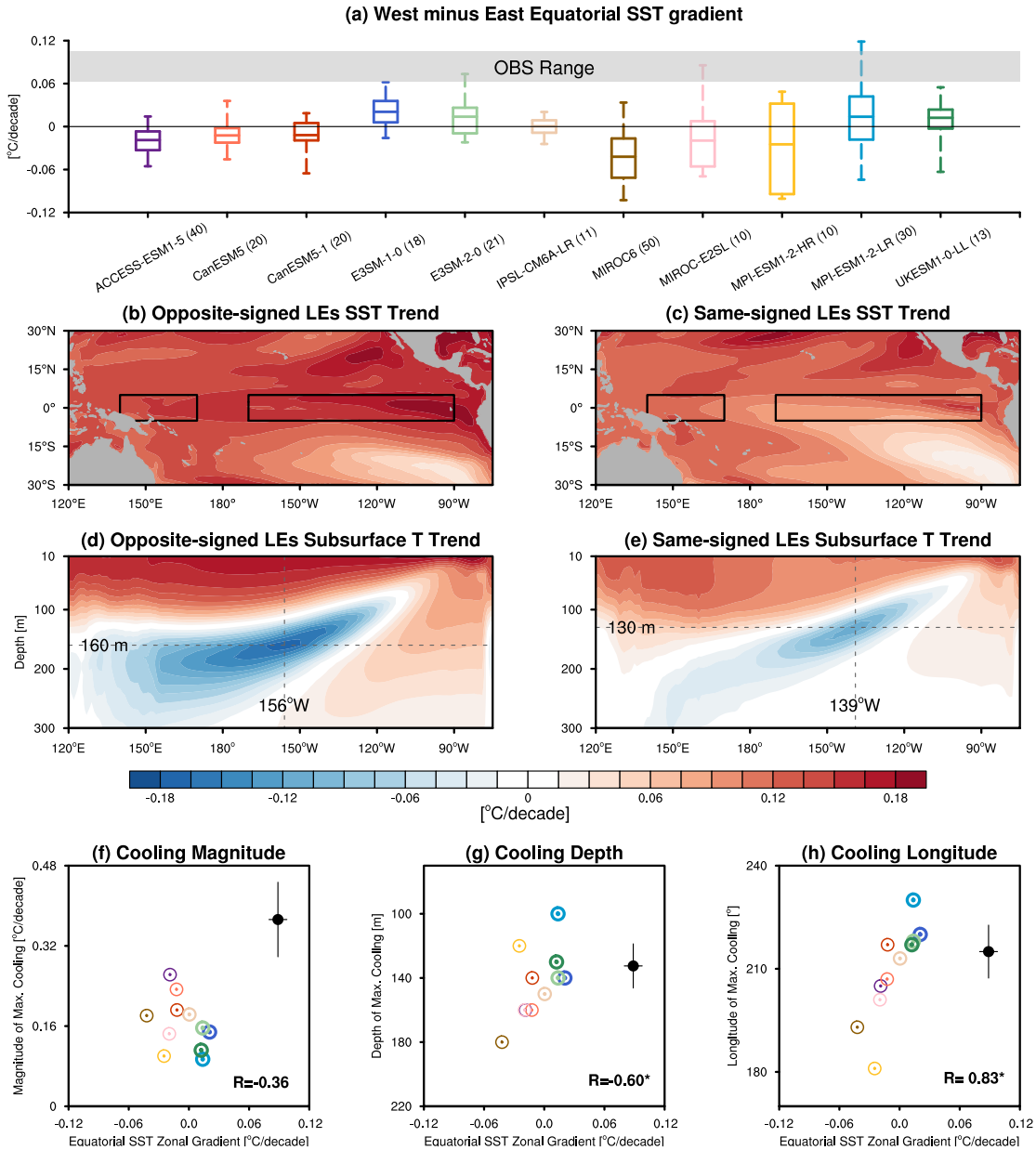

Figure 2. Relationship between sea surface temperature (SST) trend and subsurface cooling in Large Ensemble (LE) simulations. (a) Equatorial (5°S ~ 5°N) zonal (west-minus-east) SST gradient trends (°C/decade) across different LEs. The box plots show the 25th and 75th percentiles of the zonal SST gradient trend which are computed across each LE members, with the median shown as the central line, and the whiskers representing the full data range for each LE. The observed range (OBS) is also shown as gray shading based on the zonal SST gradient trends in four observational data sets. The member number for each LE is labeled with the corresponding model name. Composites of forced SST trend (°C/decade) for (b) opposite-signed LEs and (c) same-signed LEs. Black boxes in (b)–(c) indicate the regions for calculating the zonal SST gradient. Composites of forced subsurface temperature trend (°C/decade) for (d) opposite-signed LEs and (e) same-signed LEs. Dashed lines in (d)–(e) indicate the depth and longitude of the maximum cooling in the tropical Pacific upper ocean. Scatterplots of forced equatorial SST zonal gradient trend (°C/decade) with (f) the magnitude of the maximum subsurface cooling trend (°C/decade), (g) the depth of the maximum subsurface cooling trend (m), and (h) the longitude of the maximum subsurface cooling trend (°). Black dots in (f)–(h) represent the observational composites, with error bars indicating one standard deviation, based on estimates from four observational SST data sets for the *x*-axis and four observational and reanalysis subsurface temperature data sets for the *y*-axis and models are color coded as in (a). Same-signed models are represented by circumpuncts with thicker outlines, whereas opposite-signed models have thinner outlines and IPSL-CM61-LR with a near-zero SST gradient is shown with an intermediate thickness. The correlation coefficients (R) are also shown for (f)–(h) with asterisks indicating significant correlations at the 95% confidence level.

intensity (Figure 3c and Figure S3g–j in Supporting Information S1). The weaker wind stress strengthening west of 140°W and stronger weakening east of 140°W in the same-signed models (Figure 3d) accounts for the less pronounced forced response in Ekman pumping (Figure 3e) and, consequently, weaker subsurface cooling

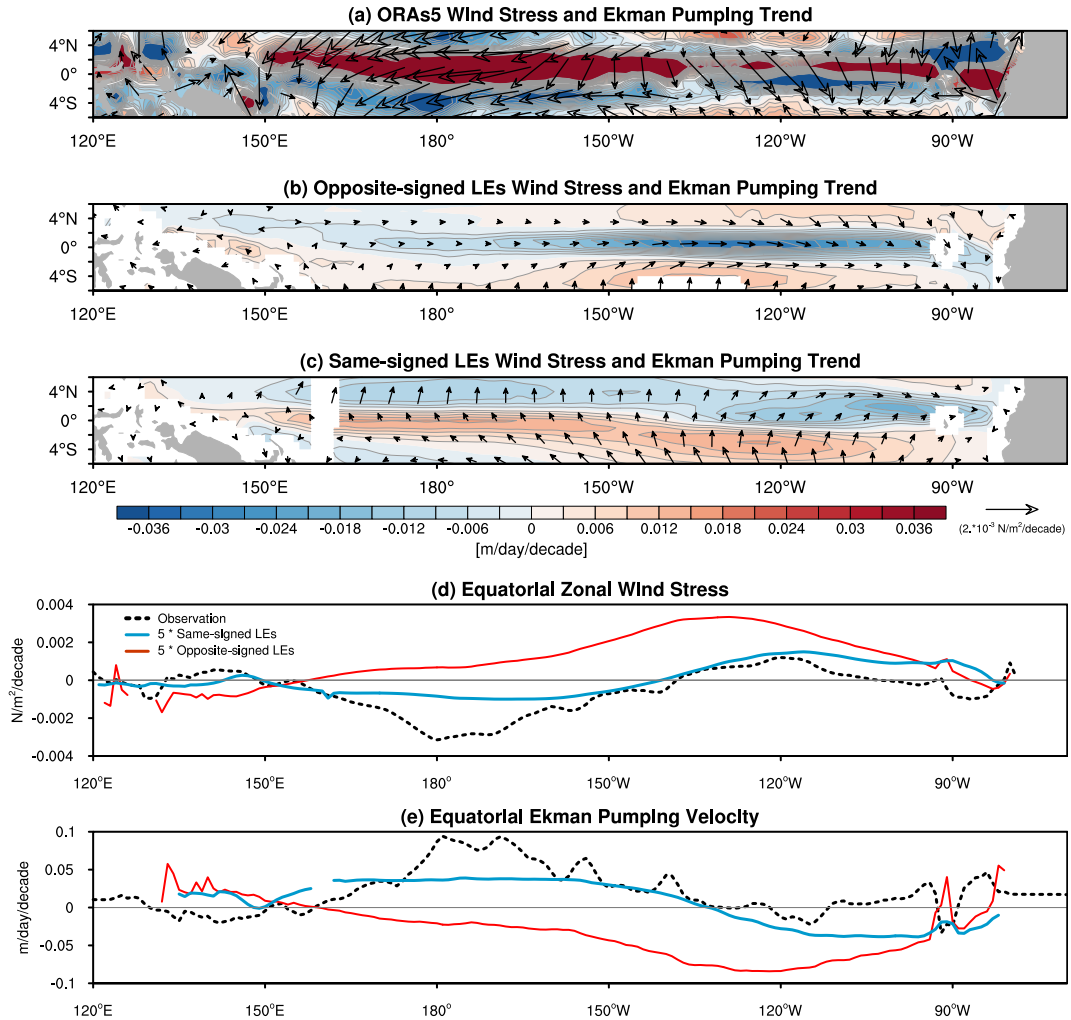

Figure 3. Trend in Ekman pumping change for observation and Large Ensemble (LE) simulations. (a) Trend in the ORAs5 wind stress (vector; N/m^2 per decade) and Ekman pumping velocity (shading; m/day per decade), (b) similar to (a) but for the composites of opposite-signed LEs, (c) similar to (a) but for the composites of same-signed LEs, and (d)–(e) meridional-mean (2°S ~ 2°N) zonal wind stress (N/m^2 per decade) and Ekman pumping velocity (m/day per decade) for ORAs5, same-signed and opposite-signed LEs.

(Figure 2f) compared to the observations. It is noted that these models reproduce the sign of the zonal wind stress trends across the equatorial Pacific and its associated upwelling change, but they do so as part of a Southern to Northern Hemisphere meridional flow that is quite distinct from the observed flow: the meridional wind stress trend in ORAs5 is from north to south in the central and eastern Pacific.

Changes in surface wind stress also drive significant variations in the equatorial zonal current. In ORAs5, the westward South Equatorial Current (SEC) weakens in the surface mixed layer and upper thermocline except in the far eastern basin, whereas east of the dateline the eastward Equatorial Undercurrent (EUC) weakens in the lower thermocline (Figure 4a). As shown in Jiang et al. (2024a), the weakening SEC in the west despite locally increased easterly wind stress is accounted for by changes in the geostrophic flow. EUC weakening has been shown to contribute weakly to thermocline cooling in the eastern equatorial Pacific (Jiang et al., 2024b). Beyond dynamical advection, these changes in zonal currents can also influence local mixing processes, thereby affecting subsurface ocean temperatures. In the central-to-eastern equatorial Pacific, the climatological westward surface SEC and eastward EUC (contour in Figure 4a) generate a strong vertical shear (contour in Figure 4b) above the thermocline, which facilitates intense mixing despite the existence of a large stabilizing vertical temperature gradient (Gregg et al., 1985; Moum et al., 1986). The vertical mixing redistributes the heat absorbed at the surface

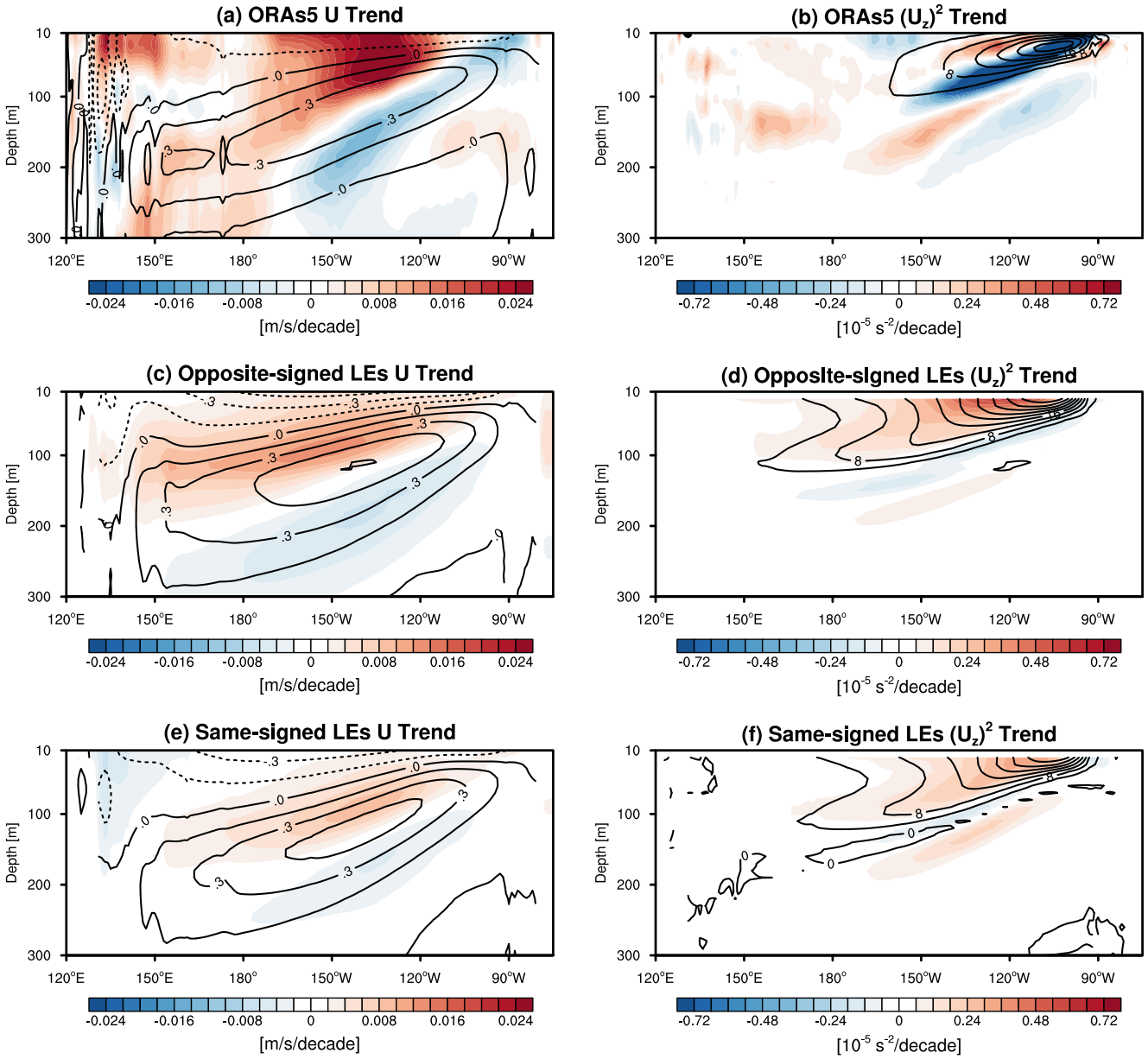

Figure 4. Trend in zonal current and its vertical shear for observation and Large Ensemble (LE) simulations. Meridional-mean (2°S ~ 2°N) zonal current trend (shadings; m/s/decade) and climatology (contours; m/s) in (a) ORAs5, (c) Opposite-signed LEs, and (e) Same-signed LEs. Meridional-mean (2°S ~ 2°N) squared vertical shear of the zonal current $\left(\frac{\partial U}{\partial z}\right)^2$ (denoted as $(U_z)^2$)) trend (10^{-5} s^{-2}/decade) and climatology (10^{-5} s^{-2}) in (b) ORAs5, (d) Opposite-signed LEs, and (f) Same-signed LEs.

downward and lifts cold water upward, counteracting advective cooling in the subsurface upper ocean (Liu et al., 2005; Ray et al., 2018a, 2018b; C. Yang et al., 2014) and cooling above contributing to the formation and maintenance of the cold tongue (Deppenmeier et al., 2022; Holmes et al., 2019). In ORAs5, the weakening of both the westward SEC and eastward EUC reduces the vertical shear of zonal currents. Since the parameterized vertical mixing in most parameterization schemes is closely related to the squared vertical shear of the horizontal current (Bernard et al., 2006; Blanke & Delecluse, 1993), the reduction in $\left(\frac{\partial U}{\partial z}\right)^2$ in the shallow thermocline over the eastern Pacific (Figure 4b) leads to decreased local mixing and subsurface cooling. Additionally, increased current shear is noted in the surface mixed layer over the eastern Pacific, possibly due to the maximum weakening of the westward current beneath the mixed layer (Figure 4a).

The vertical distributions of zonal current trend in opposite-signed and same-signed LEs (Figures 4c–4f and Figure S4 in Supporting Information S1) are both characterized with acceleration in the upper portion of EUC and deceleration in the lower portion. This is despite the fact that opposite-signed and same-signed models have distinct surface wind stress trend pattern across equatorial Pacific. It suggests that zonal current changes in LE model simulations are more likely driven by thermodynamical responses to SST changes (Peng et al., 2022; Saenko et al., 2011), instead of dynamical responses to local wind stress changes, as seen in ORAs5 where SST changes are weak in the central-to-eastern equatorial Pacific. The eastward current trend in the LE simulations occurs at greater depths than in ORAs5, primarily strengthening the upper portion of the EUC rather than weakening the SEC. Therefore the observed region of strong negative squared shear trend from 100 m depth at 150°W to the surface at 90°W is largely absent in both model groups. Consequently, the impact of current shear changes on local mixing processes and associated temperature changes is smaller in the models. It is worth noting that the positive squared shear trend in the upper layers of the same-signed models is relatively weaker and more confined to east of 120°W (Figure 4f), corresponding to the region of strong SST warming in the far eastern Pacific (Figure 2c). In contrast, the positive shear trend extends beyond 150°W in the opposite-signed models (Figure 4d), coincident with the more westward-extended warming (Figure 2b). The climatological model biases toward equatorial currents and shear that are too strong are less pronounced in the same-signed models than in the opposite-signed models. However, caution is warranted as ORAs5 may underestimate real-world climatological current velocities based on in-situ data (Johnson et al., 2001, 2002; Stellema et al., 2022).

In the opposite-signed models, the equatorial westerly anomalies favor decreased wind-driven surface layer divergence and reduced subsurface ocean convergence (Figure 5c); that is, the equatorial cell weakens (Figure 5d). Climatologically, the meridional currents and their associated MOC warm the subsurface ocean and cool the surface layer in the equatorial Pacific. Therefore, a weakening equatorial cell in opposite-signed models contributes to subsurface cooling and surface warming. In contrast, the same-signed models show a weakening of the surface northward meridional current in the Northern Hemisphere, with no consistent changes observed in the Southern Hemisphere or subsurface ocean (Figure 5e). This is accompanied by a weakening of the MOC in the Northern Hemisphere (Figure 5f). These changes are unlikely to significantly impact subsurface temperature changes at the depth of ∼130 m (Figure 2e). Given that the zonal-mean Ekman pumping changes in the same-signed models are near zero across the equatorial Pacific (Figure 3e), the changes in surface meridional current and MOC (Figures 5e and 5f) must be related to the change in the surface geostrophic component. Neither group of models realistically reproduces the observed MOC trend, which is characterized by a general strengthening of the STC in the off-equatorial regions but a weakening of the equatorial cell, particularly in the South Pacific (Figures 5a and 5b).

5. Connection Between Subsurface Temperature and SST Pattern Formation

In the eastern equatorial Pacific (approximately east of 140°W), a direct connection between the shallow thermocline and the surface mixed layer can be expected in the presence of strong climatological upwelling. In ORAs5 and the same-signed models, the shallow subsurface cooling in the eastern Pacific can affect the surface layer dominantly through enhanced thermocline feedback. Although Ekman pumping velocity decreases at the equator, which would tend to warm the surface, this effect is likely offset by cooling due to mean upwelling of colder subsurface waters (Figures 3a and 3c). In contrast, the opposite-signed models exhibit reduced upwelling and subsurface warming in the eastern Pacific, which collectively contributes to warming of the cold tongue SST.

Further west, in the central-to-eastern Pacific (approximately west of 140°W), there is increased upwelling and subsurface cooling in ORAs5 and the same-signed models, which contribute to the surface lack-of-warming through enhanced Ekman pumping and strengthened thermocline feedback. In the opposite-signed models, the pronounced thermocline cooling, however, has limited impact on the surface layer, likely due to two reasons. First, the Ekman pumping decreases due to weakening of zonal wind stress, counteracting the cooling effects due to enhanced thermocline feedback. Besides, the change in the mixing process also contributes to the ocean temperature change. In the upper ocean over the central-to-eastern Pacific, the active mixing processes, facilitated by the weakly stratified temperature structure and persistent vertical shear between the surface westward current and the eastward EUC, also play an essential role in linking the thermocline anomalies with the surface mixed layer (Deppenmeier et al., 2021, 2022; Holmes et al., 2019).

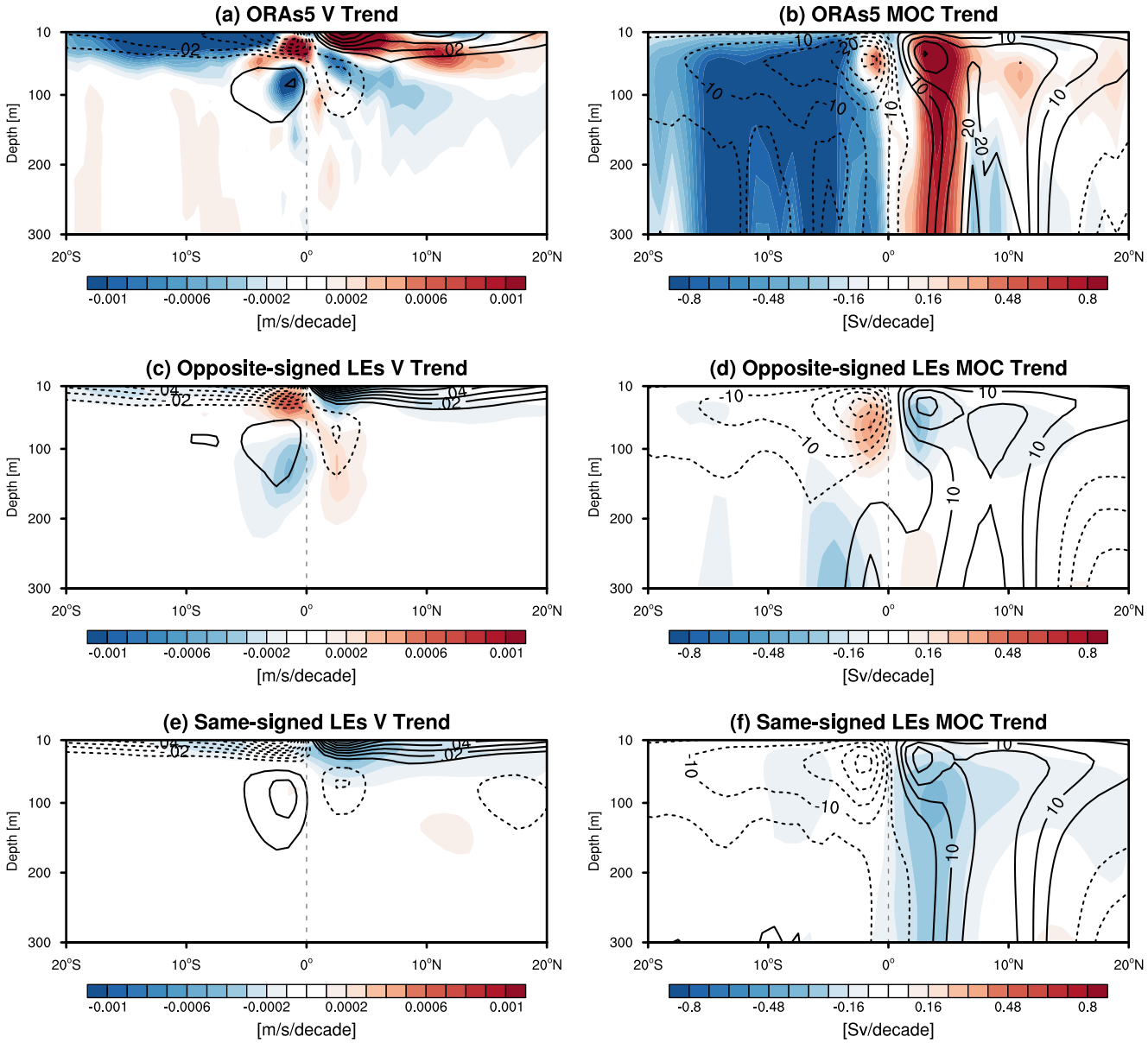

Figure 5. Trend in meridional current and Meridional Overturning Circulation (MOC) change for observation and Large Ensemble (LE) simulations. Trend (shading; m/s/decade) and climatology (contour; m/s) of zonal-mean (150°E ~ 90°W) meridional current for (a) ORAs5, (c) opposite-signed LEs and, (e) same-signed LEs. Trend (shading; Sv/decade) and climatology (contour; Sv) of MOC for, (b) ORAs5, (d) opposite-signed LEs, and (f) same-signed LEs.

We further assess potential changes in mixing by calculating the gradient Richardson number using monthly temperature, salinity, and ocean circulation data from ORAs5 and model outputs. It should be noted that the Richardson number is optimally estimated using data sets on much finer temporal and spatial timescales. Here, we estimate the Richardson number using monthly data sets under the assumption that the mixing processes can be effectively parameterized and that the upscaling applied is valid.

As detailed in the method section, trends in the gradient Richardson number depend not only on trends in square of buoyancy frequency and current shear but also on their climatological states. Figure S6 in Supporting Information S1 illustrates that climatological distributions of the Richardson number exhibit consistent characteristics across ORAs5 and LE model simulations with minima in the surface mixed layer and near the thermocline, which is indicative of strong instability and vigorous mixing. However, the magnitude of the Richardson number differs significantly across ORAs5 and different models. To facilitate comparisons between observations and models,

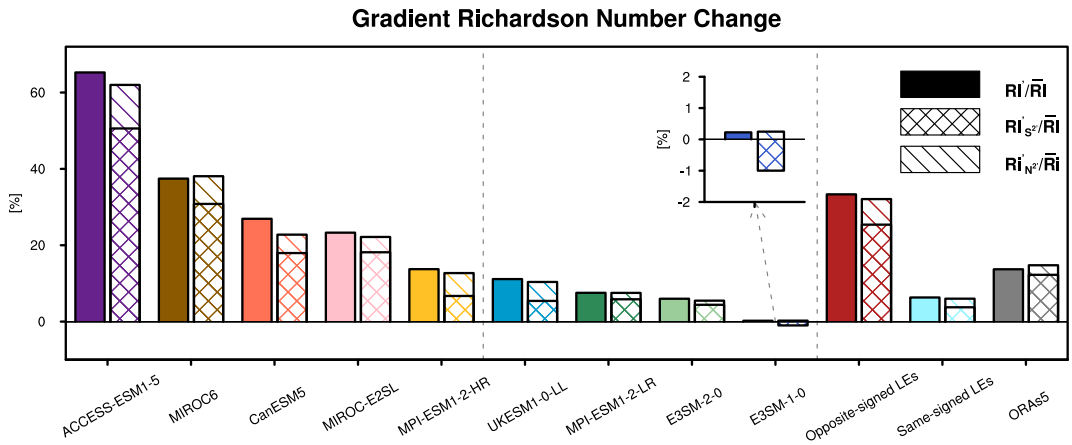

Figure 6. Changes (%) in volume-averaged normalized gradient Richardson number ratio ($Ri'/\overline{Ri}$) across opposite-signed and same-signed Large Ensemble (LE) models and ORAs5 in the upper equatorial Pacific Ocean (0 ~ 250 m, 2°S ~ 2°N, 150°E ~ 90°W). From left to right, it shows $Ri'/\overline{Ri}$ (solid bars), as well as contributions from $S^{2'}$ ($Ri'_{S^{2'}}$, crossed bars) and contributions from $N^{2'}$ ($Ri'_{N^{2'}}$, stippled bars) in individual LE models listed in the order of changes in the Richardson number ratio from largest to smallest. It also shows averaged values for both groups of LE models and ORAs5 on the right. An inset shows values for E3SM-1-0 on a different scale for clearer visualization.

and across different LE models, we in Figure 6 show the volume-averaged normalized Richardson number ($Ri'/\overline{Ri}$) for opposite-signed models, same-signed models and ORAs5 in the upper equatorial Pacific Ocean. Opposite-signed models (on the left of Figure 6), in particular, show a pronounced increase in $Ri'/\overline{Ri}$, indicating decreased vertical mixing in the upper equatorial Pacific Ocean. In contrast, the increase in $Ri'/\overline{Ri}$ is much weaker in same-signed models (at the center of Figure 6), and it is near-zero in E3SM-1-0, the model with the strongest increase in zonal SST gradient. In ORAs5, $Ri'/\overline{Ri}$ is weaker than opposite-signed models but stronger than same-signed models in the upper equatorial Pacific (on the right of Figure 6).

We further decompose $Ri'/\overline{Ri}$ into contributions from changes in shear square ($Ri'_{S^{2'}}$) and buoyancy frequency ($Ri'_{N^{2'}}$) based on Equation 6. The breakdown shows that these two factors together approximate the total $Ri'/\overline{Ri}$ in models and ORAs5 (Figure 6). In opposite-signed models, changes in both current shear and buoyancy significantly influence $Ri'/\overline{Ri}$, with shear changes exerting a greater influence than buoyancy changes. Increases in N^2 and decreases in S^2 across the equatorial Pacific upper ocean lead to the significantly increased stability in the upper ocean of opposite-signed models. This can prevent subsurface cooling from being effectively communicated to the surface layers especially in the central Pacific where climatological upwelling is weak. In same-signed models and ORAs5, change in the current shear is also the main driver of $Ri'/\overline{Ri}$.It is worth noting that in ORAs5, the shear-driven reduction in the normalized Richardson number ($Ri'_{S^{2'}}/\overline{Ri}$) primarily occurs in the eastern equatorial Pacific east of 150°W near the thermocline (not shown), contributing to localized subsurface cooling. However, this subsurface cooling appears able to affect the surface layers in the presence of strong climatological upwelling.

6. Discussion

Although we present the different mechanisms driving subsurface cooling and its connection to SST pattern formation in observations and model simulations, a closed heat budget analysis in the upper tropical Pacific Ocean remains challenging for both reanalyzes and CMIP-like model simulations, especially in the context that mixing processes cannot be quantifiably assessed with the available data. Moreover, it remains unclear why model simulations diverge so significantly from observed trends. One possibility is that the models tend to simulate stronger surface warming compared to observations, related to overestimated climate sensitivity (Lindzen & Choi, 2011; Masters, 2014). As shown in Figure 7a, the equatorial Pacific SST trend is positively correlated with the global ocean warming rate across the models ($R = 0.86$, significant at the 95% confidence level). Observational data sets show weaker equatorial Pacific and global ocean warming rates than any of the

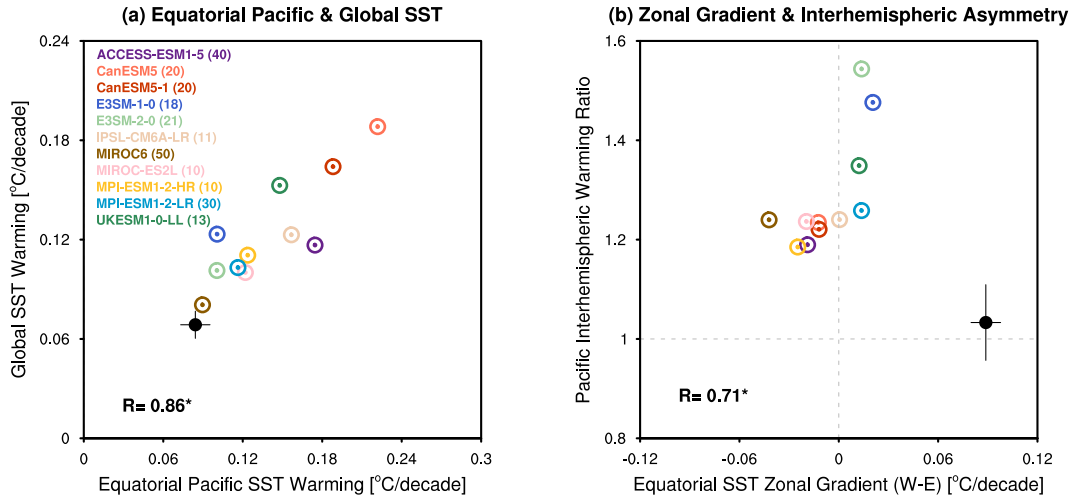

Figure 7. Relationship between equatorial Pacific sea surface temperature (SST) warming with global SST warming and Pacific Interhemispheric warming ratio. (a) Scatterplot of the forced equatorial Pacific (5°S ~ 5°N, 120°E ~ 90°W) SST trend (℃/decade) with the global SST trend (℃/decade) across Large Ensembles (LEs), (b) Scatterplot of the forced equatorial (5°S ~ 5°N) SST gradient with the interhemispheric warming asymmetry across LEs. The interhemispheric warming asymmetry is defined as the ratio of the area-weighted SST trend in the northern tropical Pacific (0° ~ 30°N, 120°E ~ 75°W) and the trend in the southern tropical Pacific (30°S ~ 0°, 120°E ~ 75°W). Black dots in (a)–(b) represent the observational composites, with error bars indicating one standard deviation based on estimates from four observational SST data sets. The correlation coefficients (R) are also shown for (a)–(b) with asterisks indicating significant correlations at the 95% confidence level.

models during the historical period. Models with stronger surface warming and the associated increases in stratification may reduce the effectiveness of the ODT mechanism by weakening the connection between thermocline cooling and SST pattern. However, there is not a strong correlation between the amount of SST warming in the tropical Pacific or globally and whether models are opposite-sign or same-sign (not shown) so this is not the only cause. A possibly related reason is that models misrepresent the coupled dynamics of the forced response. In theory, both atmospheric dynamics (Knutson & Manabe, 1995; Meehl & Washington, 1996; Vecchi et al., 2006; Vecchi & Soden, 2007)—slowing down the Walker circulation and weakening the zonal SST gradient in the tropical Pacific—and the ODT mechanism (Cane et al., 1997; Clement et al., 1996; Karnauskas et al., 2009; Seager & Murtugudde, 1997)—enhancing cooling by vertical ocean upwelling and strengthening the zonal SST gradient—are simultaneously at play in shaping the tropical Pacific's response to radiative forcing (DiNezio et al., 2010; Heede et al., 2020). Observations of the historical lack of warming in the cold tongue regions suggest that the ODT mechanism likely outweighs the counteracting atmospheric processes. In model simulations, however, the ODT mechanism appears to be less effective, possibly due to increasing upper-ocean stratification damping its role in the SST pattern formation. Models with overestimated climate sensitivity and stronger surface warming in the cold tongue region may disproportionately suppress the ODT mechanism, allowing the atmospheric warming effects to overwhelm the oceanic cooling effects in the historical period. Besides, misrepresentation of atmospheric thermodynamic effects, including the underestimated cloud radiative feedback in the southeast Pacific (Kang et al., 2023; Kim et al., 2022), can contribute to erroneous pattern formation of SST trends in climate models over the equatorial Pacific and beyond. Misrepresentations of oceanic and atmospheric processes have been linked to systematic biases in climate models, including the excessive cold tongue, the double Intertropical Convergence Zone, and unrealistically high relative humidity in the eastern Pacific that can then influence forced trends (J.-J. Luo, Liu, & Lu, 2018; Seager et al., 2019; Wills et al., 2022). However, the extent to which these biases interact, whether they compound or compensate for each other, and how they interact with the ocean dynamical processes studied here in shaping the discrepancies between simulated and observed SST patterns remains unclear.

Furthermore, although some models reproduce the same sign of the forced response over the equatorial Pacific as observed, they likely do so for different reasons. These models simulate a realistic zonal wind stress trend pattern across the equatorial Pacific, which is crucial for driving changes in ocean circulation and subsurface temperature

structure. However, the simulated zonal wind stress changes are part of a cross-equatorial flow from the Southern Hemisphere to the Northern Hemisphere associated with interhemispheric asymmetry of Pacific Ocean warming, a pattern that differs significantly from the observation (Figures 3a and 3c). As shown in Figure 7b, the forced response of the zonal SST gradient across the equatorial Pacific in LE simulations is closely linked to the interhemispheric warming asymmetry in the tropical Pacific ($R = 0.71$, significant at the 95% confidence level). All LE simulations show the northern tropical Pacific warming faster than the southern in the historical period, compared to observations, which exhibit nearly equal warming in the north and south. Moreover, the same-signed LE models show stronger asymmetric warming compared to the opposite-signed LE models. It is worth noting that the distinctively strong asymmetric warming in E3SM1 and E3SM2 may be driving the strong cross-equatorial flow (Figures S3g and h in Supporting Information S1). Hence it appears that the primary reason the same-signed models match observations is because of this erroneous preferential warming of the north tropical Pacific and the southerly flow across the equator that it drives (Fu et al., 2024; He et al., 2023). The greater than observed warming of the Northern Hemisphere oceans relative to the Southern Hemisphere oceans in models has been argued to be linked with misrepresentations of the response to radiative forcing, driven by erroneous interhemispheric differences in GHGs-induced warming and/or underestimated aerosol-driven cooling in the North Pacific (Deser et al., 2020; Friedman et al., 2013; He et al., 2023).

Throughout this study, we simplify the equatorial SST trend pattern by describing changes in the SST gradient between two predefined regions and classifying LE model simulations accordingly. However, the observed SST trend exhibits a more complex tripole-like structure, with warming in the western and far eastern equatorial Pacific and lack-of-warming in the central-to-eastern Pacific (Fu et al., 2024). A similar SST trend pattern is evident in same-signed LE models (Figure 2c). This tripole-like SST trend corresponds well to the surface zonal wind stress trend in the equatorial Pacific, which exhibits easterly anomalies in the west and westerly anomalies in the east (Figure 3d). Seager et al. (2019) linked the westerly anomalies in the east to enhanced Amazon precipitation, which weakens zonal wind stress over the eastern equatorial Pacific. Additionally, weak climatological upwelling in the far eastern equatorial and weak downwelling in the coastal equatorial Pacific (Liang et al., 2017) limit the influence of subsurface cooling on SST via thermocline feedback. Future studies should further investigate the processes shaping the fine structure of equatorial SST trends.

7. Conclusions

The observed lack of warming in the cold tongue during the historical period has been previously linked to wind-driven thermocline cooling (Jiang et al., 2024a, Jiang et al., 2024b). Although current models continue to struggle with reproducing the SST trend patterns in the equatorial Pacific, subsurface cooling is consistently evident across all LE model simulations in response to historical radiative forcing. Our findings suggest that models with deeper and westward-displaced subsurface cooling tend to simulate an opposite-signed forced response of the zonal SST gradient across the equatorial Pacific compared to observations, whereas models with shallower and eastward-displaced subsurface cooling tend to simulate the same-signed SST response.

It is important to emphasize that we do not posit different features of subsurface cooling as the sole causal origin of changes in SST gradient. Instead, we demonstrate that these different characteristics of subsurface cooling are diagnostics of the predominant mechanisms at work in observations and LE models. In Figure 8 we present schematics that illustrate the following proposed mechanisms for the subsurface cooling and its connection to SST trends.

1. The observed subsurface cooling in the central-to-eastern equatorial Pacific is primarily driven by increased Ekman pumping as a response to the strengthening of surface zonal wind stress (Figure 8a). In the eastern equatorial Pacific, where Ekman pumping decreases due to weakened wind stress, reduced vertical shear of the zonal current leads to decreases in the subsurface mixing, contributing to the local subsurface cooling. Note that the Ekman pumping change and associated subsurface cooling in the equatorial Pacific are situated within a broader context of thermocline shoaling related to wind-driven geostrophic adjustments across the tropical Pacific (Jiang et al., 2024a). The observed subsurface cooling, in turn, affects the SST trend through upwelling and strengthens the zonal SST gradient across the equatorial Pacific.
2. In the opposite-signed models, the overall weakening of zonal wind stress across the equatorial Pacific leads to decreased Ekman pumping and a weakened equatorial cell of the STC, which cools the subsurface ocean in the central-to-eastern Pacific (Figure 8b). Additionally, increases in buoyancy frequency and reductions in current

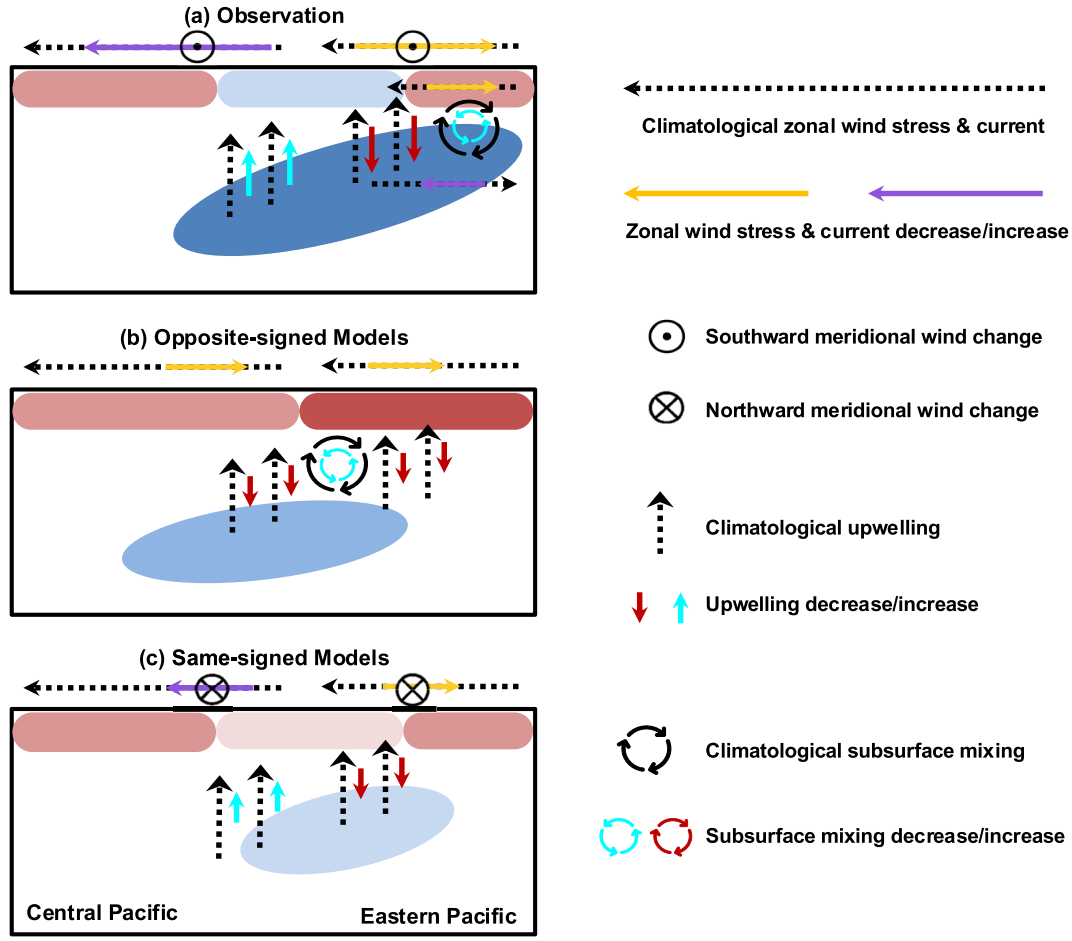

Figure 8. Schematic plot of proposed mechanisms for the subsurface cooling and its connection to sea surface temperature trend pattern formation. (a) Observation, (b) opposite-signed, and (c) same-signed models.

shear in this region enhance the Richardson number and decrease subsurface mixing, further contributing to the subsurface cooling. The increased upper ocean stability also limits the influence of this deeper and more westward-displaced subsurface cooling on the SST pattern formation by mixing between the thermocline and surface layer.

3. In the same-signed models, the zonal wind stress pattern resembles that of observations but with smaller magnitudes, resulting in weaker subsurface cooling and a correspondingly weaker strengthening of the zonal SST gradient compared to observations (Figure 8c). The changes in mixing processes are much weaker in these models compared to same-signed models. However, the zonal wind stress pattern is part of a southern to northern hemisphere flow that is opposite to that in the real world.

By addressing the different drivers of subsurface cooling in observations and climate simulations, and their connections to SST, this work has provided a more comprehensive understanding of the historical SST pattern formation in the tropical Pacific in observations and models. It is worth noting none of the models approximate the changes in the real world tropical Pacific Ocean and atmosphere and those that come closest do so for the wrong reasons.

Conflict of Interest

The authors declare no conflicts of interest relevant to this study.

Data Availability Statement

The HadISST data (Rayner et al., 2003) are located at https://metoffice.gov.uk/hadobs/hadisst/data/download.html. Kaplan SST data (Kaplan et al., 1998) are located at https://psl.noaa.gov/data/gridded/data.kaplan_sst.html. COBE SST data (Ishii et al., 2005) are located at https://psl.noaa.gov/data/gridded/data.cobe.html. ERSSTv5 SST data (Huang et al., 2017) are located at https://psl.noaa.gov/data/gridded/data.noaa.ersst.v5.html. The ORAs5 subsurface temperature, salinity, and ocean current data (Zuo et al., 2019) are located at https://cds.climate.copernicus.eu/cdsapp#!/dataset/reanalysis-oras5?tab=overview. The Ishii subsurface temperature data (Ishii & Kimoto, 2009) are located at https://rda.ucar.edu/datasets/ds285.3/. The EN4 subsurface temperature data (Good et al., 2013) is located at https://www.metoffice.gov.uk/hadobs/en4/download-en4-2-2.html. The SODA subsurface temperature data (Carton & Giese, 2008) are located at https://apdrc.soest.hawaii.edu/datadoc/soda_2.2.4.php. The LEs outputs (Deser et al., 2020) are located at https://esgf-node.ipsl.upmc.fr/search/cmip6-ipsl/.

Acknowledgments
This work was supported by NSF award OCE-2219829. RS and NGB also received additional support from NSF award AGS-2217618 and DOE award DESC0023333. CK was supported by NSF award OCE-2219830.

References

Bernard, B., Madec, G., Penduff, T., Molines, J.-M., Treguier, A.-M., Le Sommer, J., et al. (2006). Impact of partial steps and momentum advection schemes in a global ocean circulation model at eddy-permitting resolution. *Ocean Dynamics*, *56*(5–6), 543–567. https://doi.org/10.1007/s10236-006-0082-1

Blanke, B., & Delecluse, P. (1993). Variability of the tropical Atlantic ocean simulated by a general circulation model with two different mixed-layer physics. *Journal of Physical Oceanography*, *23*(7), 1363–1388. https://doi.org/10.1175/1520-0485(1993)023<1363:VOTTAO>2.0.CO;2

Cane, M. A., Clement, A. C., Kaplan, A., Kushnir, Y., Pozdnyakov, D., Seager, R., et al. (1997). Twentieth-Century sea surface temperature trends. *Science*, *275*(5302), 957–960. https://doi.org/10.1126/science.275.5302.957

Carton, J. A., & Giese, B. S. (2008). A reanalysis of ocean climate using Simple Ocean Data Assimilation (SODA). *Monthly Weather Review*, *136*(8), 2999–3017. https://doi.org/10.1175/2007MWR1978.1

Chung, E.-S., Timmermann, A., Soden, B. J., Ha, K.-J., Shi, L., & John, V. O. (2019). Reconciling opposing Walker circulation trends in observations and model projections. *Nature Climate Change*, *9*(5), 405–412. https://doi.org/10.1038/s41558-019-0446-4

Clement, A. C., Seager, R., Cane, M. A., & Zebiak, S. E. (1996). An Ocean dynamical thermostat. *Journal of Climate*, *9*(9), 2190–2196. https://doi.org/10.1175/1520-0442(1996)009<2190:AODT>2.0.CO;2

Coats, S., & Karnauskas, K. B. (2018). A role for the equatorial undercurrent in the Ocean dynamical thermostat. *Journal of Climate*, *31*(16), 6245–6261. https://doi.org/10.1175/JCLI-D-17-0513.1

Deppenmeier, A.-L., Bryan, F. O., Kessler, W. S., & Thompson, L. (2021). Modulation of cross-isothermal velocities with ENSO in the tropical pacific cold tongue. *Journal of Physical Oceanography*, *51*(5), 1559–1574. https://doi.org/10.1175/JPO-D-20-0217.1

Deppenmeier, A.-L., Bryan, F. O., Kessler, W. S., & Thompson, L. (2022). Diabatic upwelling in the tropical pacific: Seasonal and subseasonal variability. *Journal of Physical Oceanography*, *52*(11), 2657–2668. https://doi.org/10.1175/JPO-D-21-0316.1

Deser, C., Lehner, F., Rodgers, K. B., Ault, T., Delworth, T. L., DiNezio, P. N., et al. (2020). Insights from Earth system model initial-condition large ensembles and future prospects. *Nature Climate Change*, *10*(4), 277–286. https://doi.org/10.1038/s41558-020-0731-2

DiNezio, P., Clement, A., & Vecchi, G. (2010). Reconciling differing views of tropical pacific climate change. *Eos, Transactions American Geophysical Union*, *91*(16), 141–142. https://doi.org/10.1029/2010EO160001

Eyring, V., Bony, S., Meehl, G. A., Senior, C. A., Stevens, B., Stouffer, R. J., & Taylor, K. E. (2016). Overview of the Coupled Model Intercomparison Project Phase 6 (CMIP6) experimental design and organization. *Geoscientific Model Development*, *9*(5), 1937–1958. https://doi.org/10.5194/gmd-9-1937-2016

Friedman, A. R., Hwang, Y.-T., Chiang, J. C. H., & Frierson, D. M. W. (2013). Interhemispheric temperature asymmetry over the twentieth century and in future projections. *Journal of Climate*, *26*(15), 5419–5433. https://doi.org/10.1175/JCLI-D-12-00525.1

Fu, S., Hu, S., Zheng, X.-T., McMonigal, K., Larson, S., & Tian, Y. (2024). Historical changes in wind-driven ocean circulation drive pattern of Pacific warming. *Nature Communications*, *15*(1), 4190. https://doi.org/10.1038/s41467-024-48299-w

Good, S. A., Martin, M. J., & Rayner, N. A. (2013). EN4: Quality controlled ocean temperature and salinity profiles and monthly objective analyses with uncertainty estimates. *Journal of Geophysical Research: Oceans*, *118*(12), 6704–6716. https://doi.org/10.1002/2013JC009067

Gregg, M. C., Peters, H., Wesson, J. C., Oakey, N. S., & Shay, T. J. (1985). Intensive measurements of turbulence and shear in the equatorial undercurrent. *Nature*, *318*(6042), 140–144. https://doi.org/10.1038/318140a0

He, C., Clement, A. C., Kramer, S. M., Cane, M. A., Klavans, J. M., Fenske, T. M., & Murphy, L. N. (2023). Tropical Atlantic multidecadal variability is dominated by external forcing. *Nature*, *622*(7983), 521–527. https://doi.org/10.1038/s41586-023-06489-4

Heede, U. K., & Fedorov, A. V. (2021). Eastern equatorial Pacific warming delayed by aerosols and thermostat response to CO2 increase. *Nature Climate Change*, *11*(8), 696–703. https://doi.org/10.1038/s41558-021-01101-x

Heede, U. K., Fedorov, A. V., & Burls, N. J. (2020). Time scales and mechanisms for the tropical pacific response to global warming: A tug of war between the Ocean thermostat and weaker walker. *Journal of Climate*, *33*(14), 6101–6118. https://doi.org/10.1175/jcli-d-19-0690.1

Holmes, R. M., Zika, J. D., & England, M. H. (2019). Diathermal heat transport in a global ocean model. *Journal of Physical Oceanography*, *49*(1), 141–161. https://doi.org/10.1175/JPO-D-18-0098.1

Huang, B., Thorne, P. W., Banzon, V. F., Boyer, T., Chepurin, G., Lawrimore, J. H., et al. (2017). Extended Reconstructed Sea Surface Temperature, version 5 (ERSSTv5): Upgrades, validations, and intercomparisons. *Journal of Climate*, *30*(20), 8179–8205. https://doi.org/10.1175/JCLI-D-16-0836.1

Ishii, M., & Kimoto, M. (2009). Reevaluation of historical ocean heat content variations with time-varying XBT and MBT depth bias corrections. *Journal of Oceanography*, *65*(3), 287–299. https://doi.org/10.1007/s10872-009-0027-7

Ishii, M., Shouji, A., Sugimoto, S., & Matsumoto, T. (2005). Objective analyses of sea-surface temperature and marine meteorological variables for the 20th century using ICOADS and the Kobe Collection. *International Journal of Climatology*, *25*(7), 865–879. https://doi.org/10.1002/joc.1169

Jiang, F., Seager, R., & Cane, M. A. (2024a). A climate change signal in the tropical Pacific emerges from decadal variability. *Nature Communications*, *15*(1), 8291. https://doi.org/10.1038/s41467-024-52731-6

Jiang, F., Seager, R., & Cane, M. A. (2024b). Historical subsurface cooling in the tropical pacific and its dynamics. *Journal of Climate*, *37*(22), 5925–5938. https://doi.org/10.1175/JCLI-D-24-0007.1

Johnson, G. C., McPhaden, M. J., & Firing, E. (2001). Equatorial Pacific Ocean horizontal velocity, divergence, and upwelling. *Journal of Physical Oceanography*, *31*(3), 839–849. https://doi.org/10.1175/1520-0485(2001)031<0839:EPOHVD>2.0.CO;2

Johnson, G. C., Sloyan, B. M., Kessler, W. S., & McTaggart, K. E. (2002). Direct measurements of upper ocean currents and water properties across the tropical Pacific during the 1990s. *Progress in Oceanography*, *52*(1), 31–61. https://doi.org/10.1016/S0079-6611(02)00021-6

Ju, W., Zhang, Y., & Du, Y. (2022). Subsurface cooling in the tropical pacific under a warming climate. *Journal of Geophysical Research: Oceans*, *127*(5), e2021JC018225. https://doi.org/10.1029/2021JC018225

Kang, S. M., Ceppi, P., Yu, Y., & Kang, I.-S. (2023). Recent global climate feedback controlled by Southern Ocean cooling. *Nature Geoscience*, *16*(9), 775–780. https://doi.org/10.1038/s41561-023-01256-6

Kaplan, A., Cane, M. A., Kushnir, Y., Clement, A. C., Blumenthal, M. B., & Rajagopalan, B. (1998). Analyses of global sea surface temperature 1856–1991. *Journal of Geophysical Research*, *103*(C9), 18567–18589. https://doi.org/10.1029/97JC01736

Karamperidou, C., Jin, F.-F., & Conroy, J. L. (2017). The importance of ENSO nonlinearities in tropical pacific response to external forcing. *Climate Dynamics*, *49*(7–8), 2695–2704. https://doi.org/10.1007/s00382-016-3475-y

Karnauskas, K. B., Seager, R., Kaplan, A., Kushnir, Y., & Cane, M. A. (2009). Observed strengthening of the zonal sea surface temperature gradient across the equatorial Pacific Ocean. *Journal of Climate*, *22*(16), 4316–4321. https://doi.org/10.1175/2009JCLI2936.1

Kim, H., Kang, S. M., Kay, J. E., & Xie, S.-P. (2022). Subtropical clouds key to Southern Ocean teleconnections to the tropical Pacific. *Proceedings of the National Academy of Sciences*, *119*(34), e2200514119. https://doi.org/10.1073/pnas.2200514119

Knutson, T. R., & Manabe, S. (1995). Time-mean response over the tropical pacific to increased CO_2 in a coupled ocean-atmosphere model. *Journal of Climate*, *8*(9), 2181–2199. https://doi.org/10.1175/1520-0442(1995)008<2181:TMROTT>2.0.CO;2

Lee, S., L'Heureux, M., Wittenberg, A. T., Seager, R., O'Gorman, P. A., & Johnson, N. C. (2022). On the future zonal contrasts of equatorial Pacific climate: Perspectives from Observations, Simulations, and Theories. *NPJ Climate and Atmospheric Science*, *5*(1), 82. https://doi.org/10.1038/s41612-022-00301-2

Li, G., Cheng, L., Zhu, J., Trenberth, K. E., Mann, M. E., & Abraham, J. P. (2020). Increasing ocean stratification over the past half-century. *Nature Climate Change*, *10*(12), 1116–1123. https://doi.org/10.1038/s41558-020-00918-2

Liang, X., Spall, M., & Wunsch, C. (2017). Global Ocean vertical velocity from a dynamically consistent ocean state estimate. *Journal of Geophysical Research: Oceans*, *122*(10), 8208–8224. https://doi.org/10.1002/2017JC012985

Lindzen, R. S., & Choi, Y.-S. (2011). On the observational determination of climate sensitivity and its implications. *Asia-Pacific Journal of Atmospheric Sciences*, *47*(4), 377–390. https://doi.org/10.1007/s13143-011-0023-x

Liu, Z., Vavrus, S., He, F., Wen, N., & Zhong, Y. (2005). Rethinking tropical ocean response to global warming: The enhanced equatorial warming. *Journal of Climate*, *18*(22), 4684–4700. https://doi.org/10.1175/JCLI3579.1

Luo, J.-J., Wang, G., & Dommenget, D. (2018). Common model biases reduce CMIP5's ability to simulate the recent Pacific La Niña-like cooling? *Climate Dynamics*, *50*(3–4), 1335–1351. https://doi.org/10.1007/s00382-017-3688-8

Luo, Y., Liu, F., & Lu, J. (2018). Response of the equatorial Pacific thermocline to climate warming. *Ocean Dynamics*, *68*(11), 1419–1429. https://doi.org/10.1007/s10236-018-1209-x

Luo, Y., & Rothstein, L. M. (2011). Response of the Pacific Ocean circulation to climate change. *Atmosphere-Ocean*, *49*(3), 235–244. https://doi.org/10.1080/07055900.2011.602325

Luo, Y., Rothstein, L. M., & Zhang, R. (2009). Response of Pacific subtropical-tropical thermocline water pathways and transports to global warming. *Geophysical Research Letters*, *36*(4), 2008GL036705. https://doi.org/10.1029/2008GL036705

Masters, T. (2014). Observational estimate of climate sensitivity from changes in the rate of ocean heat uptake and comparison to CMIP5 models. *Climate Dynamics*, *42*(7–8), 2173–2181. https://doi.org/10.1007/s00382-013-1770-4

Meehl, G. A., & Washington, W. M. (1996). El Niño-like climate change in a model with increased atmospheric CO2 concentrations. *Nature*, *382*(6586), 56–60. https://doi.org/10.1038/382056a0

Moum, J. N., Caldwell, D. R., Paulson, C. A., Chereskin, T. V., & Regier, L. A. (1986). Does Ocean turbulence peak at the equator? *Journal of Physical Oceanography*, *16*(11), 1991–1994. https://doi.org/10.1175/1520-0485(1986)016<1991:DOTPAT>2.0.CO;2

Munk, W. (1981). Internal waves and small scale processes. In *Evolution of physical oceanography* (pp. 264–291). MIT Press.

Olonscheck, D., Rugenstein, M., & Marotzke, J. (2020). Broad consistency between observed and simulated trends in sea surface temperature patterns. *Geophysical Research Letters*, *47*(10), e2019GL086773. https://doi.org/10.1029/2019GL086773

O'Neill, B. C., Tebaldi, C., van Vuuren, D. P., Eyring, V., Friedlingstein, P., Hurtt, G., et al. (2016). The Scenario Model Intercomparison Project (ScenarioMIP) for CMIP6. *Geoscientific Model Development*, *9*(9), 3461–3482. https://doi.org/10.5194/gmd-9-3461-2016

Peng, Q., Xie, S.-P., Wang, D., Huang, R. X., Chen, G., Shu, Y., et al. (2022). Surface warming–induced global acceleration of upper ocean currents. *Science Advances*, *8*(16), eabj8394. https://doi.org/10.1126/sciadv.abj8394

Ray, S., Wittenberg, A. T., Griffies, S. M., & Zeng, F. (2018a). Understanding the equatorial pacific cold tongue time-mean heat budget. Part I: Diagnostic framework. *Journal of Climate*, *31*(24), 9965–9985. https://doi.org/10.1175/JCLI-D-18-0152.1

Ray, S., Wittenberg, A. T., Griffies, S. M., & Zeng, F. (2018b). Understanding the equatorial pacific cold tongue time-mean heat budget. Part II: Evaluation of the GFDL-FLOR coupled GCM. *Journal of Climate*, *31*(24), 9987–10011. https://doi.org/10.1175/JCLI-D-18-0153.1

Rayner, N. A., Parker, D. E., Horton, E. B., Folland, C. K., Alexander, L. V., Rowell, D. P., et al. (2003). Global analyses of sea surface temperature, sea ice, and night marine air temperature since the late nineteenth century. *Journal of Geophysical Research*, *108*(D14), 4407. https://doi.org/10.1029/2002JD002670

Saenko, O. A., Yang, X.-Y., England, M. H., & Lee, W. G. (2011). Subduction and transport in the Indian and pacific oceans in a 2 × CO2 climate. *Journal of Climate*, *24*(6), 1821–1838. https://doi.org/10.1175/2010JCLI3880.1

Schneider, N. (2000). A decadal spiciness mode in the tropics. *Geophysical Research Letters*, *27*(2), 257–260. https://doi.org/10.1029/1999GL002348

Seager, R., Cane, M., Henderson, N., Lee, D.-E., Abernathey, R., & Zhang, H. (2019). Strengthening tropical Pacific zonal sea surface temperature gradient consistent with rising greenhouse gases. *Nature Climate Change*, *9*(7), 517–522. https://doi.org/10.1038/s41558-019-0505-x

Seager, R., Henderson, N., & Cane, M. (2022). Persistent discrepancies between observed and modeled trends in the tropical Pacific Ocean. *Journal of Climate*, *35*(14), 4571–4584. https://doi.org/10.1175/JCLI-D-21-0648.1

Seager, R., & Murtugudde, R. (1997). Ocean dynamics, thermocline adjustment, and regulation of tropical SST. *Journal of Climate*, *10*(3), 521–534. https://doi.org/10.1175/1520-0442(1997)010<0521:ODTAAR>2.0.CO;2

Stellema, A., Sen Gupta, A., Taschetto, A. S., & Feng, M. (2022). Pacific Equatorial Undercurrent: Mean state, sources, and future changes across models. *Frontiers in Climate*, *4*, 933091. https://doi.org/10.3389/fclim.2022.933091

Vecchi, G. A., & Soden, B. J. (2007). Global warming and the weakening of the tropical circulation. *Journal of Climate*, *20*(17), 4316–4340. https://doi.org/10.1175/JCLI4258.1

Vecchi, G. A., Soden, B. J., Wittenberg, A. T., Held, I. M., Leetmaa, A., & Harrison, M. J. (2006). Weakening of tropical Pacific atmospheric circulation due to anthropogenic forcing. *Nature*, *441*(7089), 73–76. https://doi.org/10.1038/nature04744

Watanabe, M., Dufresne, J.-L., Kosaka, Y., Mauritsen, T., & Tatebe, H. (2021). Enhanced warming constrained by past trends in equatorial Pacific sea surface temperature gradient. *Nature Climate Change*, *11*(1), 33–37. https://doi.org/10.1038/s41558-020-00933-3

Watanabe, M., Kang, S. M., Collins, M., Hwang, Y.-T., McGregor, S., & Stuecker, M. F. (2024). Possible shift in controls of the tropical Pacific surface warming pattern. *Nature*, *630*(8016), 315–324. https://doi.org/10.1038/s41586-024-07452-7

Wills, R. C. J., Dong, Y., Proistosecu, C., Armour, K. C., & Battisti, D. S. (2022). Systematic climate model biases in the large-scale patterns of recent sea-surface temperature and sea-level pressure change. *Geophysical Research Letters*, *49*(17), e2022GL100011. https://doi.org/10.1029/2022GL100011

Yang, C., Giese, B. S., & Wu, L. (2014). Ocean dynamics and tropical Pacific climate change in ocean reanalyses and coupled climate models. *Journal of Geophysical Research: Oceans*, *119*(10), 7066–7077. https://doi.org/10.1002/2014JC009979

Yang, H., Wang, F., & Sun, A. (2009). Understanding the ocean temperature change in global warming: The tropical pacific. *Tellus A*, *61*(3), 371–380. https://doi.org/10.1111/j.1600-0870.2009.00390.x

Zebiak, S. E., & Cane, M. A. (1987). A model El Niño–southern oscillation. *Monthly Weather Review*, *115*(10), 2262–2278. https://doi.org/10.1175/1520-0493(1987)115<2262:AMENO>2.0.CO;2

Zhang, W., Li, J., & Zhao, X. (2010). Sea surface temperature cooling mode in the Pacific cold tongue. *Journal of Geophysical Research*, *115*(C12), 2010JC006501. https://doi.org/10.1029/2010JC006501

Zuo, H., Balmaseda, M. A., Tietsche, S., Mogensen, K., & Mayer, M. (2019). The ECMWF operational ensemble reanalysis–analysis system for ocean and sea ice: A description of the system and assessment. *Ocean Science*, *15*(3), 779–808. https://doi.org/10.5194/os-15-779-2019